SEARCH FOR THE DARK PHOTON AND LOW MOMENTUM MUONS STUDY

Teena V. John
MS13040

A dissertation submitted for the partial fulfilment of BS-MS dual degree in Science

Indian Institute of Science Education and Research Mohali
April 2018

Certificate of Examination

This is to certify that the dissertation titled **SEARCH FOR THE DARK PHOTON AND LOW MOMENTUM MUONS STUDY** submitted by **Teena V. John** (Reg. No. MS13040) for the partial fulfillment of BS-MS dual degree programme of the Institute, has been examined by the thesis committee duly appointed by the Institute. The committee finds the work done by the candidate satisfactory and recommends that the report be accepted.

Dr. Ananth Venkatesan Dr. Satyajit Jena Dr. Vishal Bhardwaj

(Supervisor)

Dated: April 20, 2018

Declaration

The work presented in this dissertation has been carried out by me under the guidance of Dr. Vishal Bhardwaj at the Indian Institute of Science Education and Research Mohali.

This work has not been submitted in part or in full for a degree, a diploma, or a fellowship to any other university or institute. Whenever contributions of others are involved, every effort is made to indicate this clearly, with due acknowledgement of collaborative research and discussions. This thesis is a bonafide record of original work done by me and all sources listed within have been detailed in the bibliography.

Teena V. John
(Candidate)

Dated: April 20, 2018

In my capacity as the supervisor of the candidates project work, I certify that the above statements by the candidate are true to the best of my knowledge.

Dr. Vishal Bhardwaj
(Supervisor)

Acknowledgement

First and foremost, I would like to thank my thesis supervisor Dr. Vishal Bhardwaj for his guidance and monitoring throughout the project. The talks that I had with him has improved my capacities at an expert level. Also, I would like to thank my thesis committee members Dr. Ananth Venkatesan and Dr. Satyajit Jena for their valuable suggestions and criticism of my work.

I owe my deepest gratitude to Ph.D. students, Renu Garg and Sourav Patra, for helping me with the discussions. I am highly grateful to the Deputy Librarian, Dr. Vishaki, Library Information Assistant Mr. Shameer K. K. for their promptness and assistance.

I would like to thank all my friends for supporting and helping me during the entire period of the project. I would like to acknowledge the moral support and encouragement, that I have received from my parents.

I sincerely thank Belle Collaboration for providing necessary resources used in this project.

Finally, I would like to acknowledge IISER Mohali for providing me Infrastructure and Computer Centre for carrying out my project. I am thankful to DST INSPIRE, Government of India for supporting me with the fellowship.

List of Figures

2.1 Direct dark photon prodution process at e^+e^- colliders 9
2.2 Production process of hypothetical dark photon in D^{*0} decay at e^+e^- collider. 11
2.3 Used discriminating variables 12
2.4 Used D^0 Decay Modes 14
2.5 Visualization of the whole data set. 14
2.6 Expected background coming from generic MC sample. 15
2.7 Signal and background plots for the decay $D^{*0} \to D^0 e^+ e^-$ 16
2.8 MC comparison $D^* \to D^0 X(25)[\to e^+e^-]$ decay mode. 17
2.9 1D fit to the $M_{e^+e^-}$ distribution for different D^0 decay modes in $D^* \to D^0 X(25)$. To parameterize the signal PDF, we used sum of two Gaussians and a bifurcated Gaussian. 19
2.10 Efficiency (in %) vs D^0 decay modes. 20
2.11 1D fit to the $M_{e^+e^-}$ distribution for different dark photon masses. To parameterize the signal PDF, we used sum of two Gaussians and a bifurcated Gaussian. 21
2.12 Efficiency (in %) vs different dark photon masses 22

3.1 Muon decay feynman diagram. 23
3.2 PXD Energy Deposited at different energies 26
3.3 SVD cluster charge at different energies 27
3.4 CDC ADC count at different energies 28

A.1 Invariant mass (M_{D^0}) distribution for $D^* \to D^0 n\pi$ 31
A.2 Mass Difference($\Delta M \equiv M_{D^*} - M_{D^0}$)distribution for $D^* \to D^0 n\pi$ 32
A.3 p_{D^*} distribution for $D^* \to D^0 n\pi$ 33
A.4 $M_{e^+e^-}$ distribution for $D^* \to D^0 n\pi$ 34

B.1 $D^0 \to K^-\pi^+$ Signal MC 35

B.2 $D^0 \to K^-\pi^+\pi^0$ Signal MC 35
B.3 $D^0 \to K^-\pi^+\pi^+\pi^-$ Signal MC 36
B.4 $D^0 \to K^0_s\pi^+\pi^-$ Signal MC 36
B.5 $D^0 \to K^0_s\pi^+\pi^-\pi^0$ Signal MC 36

C.1 Invariant mass (M_{ee}) distribution for different D^0 decay modes along with the expected signal and the background 37

List of Tables

2.1 D^0 Decay Modes and its branching fraction 12
2.2 Generic MC sample explanation [1]. 13
2.3 Summarizing the expected yield of dark photons candidate for different D^0 modes using $\epsilon^2 \sim 10^{-6}$. 20

Notation

D^0	D^0 meson
D^*	D^* meson
e^-	electron
e^+	positron
μ^-	muon
μ^+	anti-muon
ν_e	electron neutrino
$\overline{\nu}_e$	electron antineutrino
ν_μ	muon neutrino
$\overline{\nu}_\mu$	muon antineutrino
ϵ	Mixing parameter
m_γ	Mass of the dark photon
α	QED fine structure constant
α'	dark coupling constant
E_{cm}	center-of-mass energy
γ	Photon
$\mathcal{B}$	Branching Ratio

Abstract

A dark photon is a well-motivated hypothetical particle. If it is found, that will be a sure New Physics (NP) beyond the Standard Model (SM). Using kinetic mixing model, one can expect to search for the dark photon using $D^* \to D^0 A'$ decay mode which has suppressed branching ratio of $\mathcal{B}(D^* \to D^0 A') = \epsilon^2 \mathcal{B}(D^* \to D^0 \gamma)$. Here ϵ^2 is expected to have value between 10^{-6} and 10^{-8}. In this MS thesis, I studied the production of $D^* \to D^0 A'$ at Belle (II) for the first time. We studied the reconstruction efficiency using different mass hypothesis for the dark photon. In order to increase the signal statistics, we include five decay modes of D^0 : $K^-\pi^+$, $K^-\pi^+\pi^0$, $K^-\pi^+\pi^+\pi^-$, $K^0_S\pi^+\pi^-$, and $K^0_S\pi^+\pi^-\pi^0$. These 5 modes cover 34% of the total D^0 modes, helping us to achieve better efficiency. We estimated signal events for each mode separately and found to be 10-35 signal events in each mode at Belle. We also studied the background using the generic MC sample. Based on this preliminary study, we expect that one can put some constraints on the dark photon model using the Belle (II) data.

In the second part of my work, efforts were directed towards the improvement of low momentum muon identification at Belle II. As the muon detector is located at the end of the Belle II detector, low momentum muons < 500 MeV are lost and left undetected. The detection of low momentum muons will increases the reach of Belle II and can help in improving the signal sensitivity of New Physics (NP) searches (such as Flavour-Changing Neutral Current and Lepton Flavour Violation). We found that at first principle one should be able to exploit inner part detectors (PXD, SVD, and CDC) to identify low momentum muons.

Contents

List of Figures ii

List of Tables iii

Notation v

Abstract vii

1 Introduction 1

2 Search for the Dark Photon 5

2.1 Observational Evidence of Dark Matter 5

2.1.1 Galaxy Clusters 5

2.1.2 Galactic Rotation curves 5

2.1.3 Gravitational Lensing 6

2.1.4 The Cosmic Microwave Background 6

2.2 Dark Photon 7

2.3 Dark Photon Model-Kinetic Mixing Model 8

2.4 Dark Photon Searches 8

2.5 Anomaly in ^8Be Nuclear Transition 9

2.6 Signal 10

2.7 Generic Monte Carlo Sample 12

2.8 Data Analysis 13

2.8.1 Event Generation 13

2.8.2 Skimming 14

2.9 Expected Background 15

2.10 Signal comparison with the background 16

2.11 Signal Efficiency 17

2.11.1 Fitting different D^0 decay modes 17

2.11.2 Efficiency in variation with mass of dark photon. 20

3 Low Momentum Muon Study at Belle II **23**

3.1 Muons 23

3.2 Muon detection in Belle II 24

3.3 Importance of low momentum muon study 24

3.4 Study 25

3.4.1 Variables Used 25

4 Results and Conclusions **29**

4.1 Future scope 30

A Signal and Background and comparison for $D^* \to D^0 e^+ e^-$ and $D^* \to D^0 X(25)[\to e^+ e^-]$ **31**

B **35**

B.1 ΔM , M_{D^0}, and $M_{e^+e^-}$ distribution for different D^0 decay modes 35

C (M_{ee}) distribution for signal and Background **37**

Bibliography **40**

Chapter 1

Introduction

Our visible Universe comprises of three types of elementary particles quarks, leptons, and bosons. These particles are the fundamental building blocks of matter. There also exists antimatter, which consists of antiparticles. According to the Big Bang theory, an equal amount of matter and antimatter were created initially. When matter and antimatter come in contact with each other, they annihilate and release energy in the form of radiation. Currently, we are surrounded only by matter which means that there is some difference between the matter and antimatter.

The distinguishing features between a particle and an antiparticle are charge and parity. Antiparticle carries the opposite charge of particles. Swapping the parity of a system gives us the mirror image of the system. Application of CP on the matter provides the mirror image of its antimatter. The strong and electromagnetic interactions are CP symmetric. Until 1964, it was believed that CP symmetry was naively held in the weak interaction. In 1964, Val Fitch, Jim Cronin, and collaborators observed the CP violation for the first time in the study of neutral kaon decay. In spite of the fact that the observed effect was minimal, the proof was critical as it demonstrated that there exists an intrinsic difference between matter and antimatter. Later in 1980, Fitch and Cronin were granted the Nobel Prize for the same[2].

In 1973, Makoto Kobayashi and Toshihide Maskawa proposed the KM-mechanism which successfully explained the CP violation by postulating the existence of a third family of quarks. There exists no experimental evidence for the third generation of quarks when the theory was proposed. The portion of CP violation that is compatible with our current understanding of the standard model isn$'$t enough to account for

the present-day absence of antimatter in the universe. In addition to this, kaons are inappropriate to model in the theory as it is held together by the strong force. It was noticed that theoretical calculation isn′t tricky with more massive quarks such as bottom quarks. As the quarks aren′t free, physicists are compelled to study the decay of composite particles which contain these quarks. The decay of B-mesons violates CP symmetry. The angles of the unitary triangle represent the amount of CP violation, and its sides are derived from the elements of Cabibbo-Kobayashi-Maskawa (CKM) matrix (which describe the relative strength of the weak decays of free quarks)[2].
B-mesons are particles composed of a bottom quark (b-quark) and quark of another flavor (u or d here). B-mesons are desirable for the study of CP violation due to the number of CP violating processes that can be observed in their decays. B-factories collide particles at the $\Upsilon(4S)$ resonance, meaning that they collide at a center of mass energy equal to the mass of the $\Upsilon(4S)$. The $\Upsilon(4S)$ has a mass higher than the energy required to create a pair of B-mesons. $\Upsilon(4S)$ particles will decay into a pair of B-mesons most of the time.
Belle detector along with the BaBar played a significant part in validating the Kobayashi Maskawa mechanism for the CP violation in the Standard Model (SM) leading to Nobel prize to Kobayashi and Maskawa in 2008. Belle II experiment is a successor of the Belle detector situated at super KEKB at KEK, Tsukuba, Japan.
Belle II is the new detector for the Super KEKB flavor factory. Various rare, suppressed in the SM process are observed by the Belle experiment. Some results are few σ away from the SM. Since the luminosity of the previous KEKB accelerator is limited, most of the hints of NP are statistically limited. The integrated luminosity of Super KEKB accelerator, the upgraded accelerator of the Belle II experiment, is about 50 times greater than that of the previous accelerator. The increased luminosity and the new components of Belle II will help in doing precision studies and we can explore different scenario beyond the SM. In the new e^+e^- collider, the beam energies for electrons is 7 GeV and for positrons is 4 GeV [3]. The components of the Belle II detectors are the following.

1. Pixel Detector (PXD)

   It is the innermost detector of the Belle II experiment. The SuperKEKB luminosity creates a large background. Since the nano-beam scheme is using in Belle II, the radius of the beam pipe around the interaction is reduced to 14 mm. This also adds to the background effect. This challenging situation is overcome by the

usage of, DEPFET (DEPleted Field Effect Transistor) technology. It performs the accurate measurement of the track positions to reconstruct the decay vertex of short living particles. The DEPFET technology enables the detector to perform signal detection and signal amplification in a single silicon pixel structure. Apart from this, pixel detector has an excellent signal to noise ratio, low power consumption, and a non-destructive read-out. The pixel detector consists of two DEPFET layers at radii 14mm and 22 mm[4].

2. Silicon Vertex Detector (SVD)

   It is also a part of the vertex detector, which is located between Pixel Detector and Central Drift Chamber. It measures the vertex information of low momentum particles which cannot propagate further to CDC. It also provides data to extrapolate the tracks reconstructed in the CDC back into the PXD with high efficiency. SVD is made up of four layers of double-sided silicon strip detectors (DSSDs)[3].

3. Central Drift Chamber (CDC)

   CDC is placed outside of SVD. It has an inner radius of 160 mm and outer radius of 1130 mm. It has a large chamber volume filled with helium-ethane gas and integrated with an upgraded wire configuration. It plays a key role in the precise reconstruction and momenta measurements of the charged tracks. When charged particle pass through the gas chamber it gets ionized, and CDC collects the data triggered by the ionization process along with the advanced algorithm. CDC also plays a role in determining the identities of various charged particles by measuring their energy loss within the gas volume[3].

4. Particle Identification System (PID)

   In the Belle II detector, PID is based on imaging the Cherenkov rings created by the passage of charged particles. It consists of two detectors-Time-Of-Propagation (TOP) counter in the central region and Aerogel Ring Imaging Cherenkov (ARICH) counter in the end cap region.

   - Time-of-Propagation (TOP) Counter
     It consists of quartz radiator bar, microchannel plate photomultipliers (MCP-PMTs), and a front-end readout. In this detector, the Cherenkov

photons emitted by a charged track in the radiator undergo total internal reflections at the quartz surface and are detected by the MCP-PMTs. The likelihood for a given particle mass hypothesis is computed using the time of flight of the charged particle, time of propagation of emitted photons and position in the detection plane of each Cherenkov photon. It provides excellent separation between kaons and pions[5].

- Aerogel Ring Imaging Cherenkov (ARICH) Detector
  It consists of aerogel radiator, and an array of position sensitive photon detectors. As the charged particle enters the radiator, it emits Cherenkov light photons to the direction which depends on the particle velocity. A new photon sensor named Hybrid Avalanche Photon Detector (HAPD) is used to collect a small number of the Cherenkov light photons distributed in the large area effectively. It distinguishes slow pion, muon, and electrons with low momentum and provides a good separation between pions and kaons[5].

5. Electromagnetic Calorimeter (ECL)

   The ECL consists of barrel part and two end caps. It measures photon energy and position, reconstructs electrically neutral particles, and detects K_L^0 along with the KLM detector. It consists of Cesium Iodide crystals (Thallium doped) which are arranged in barrel part and two end caps. When a particle moves through the crystal, it interacts with the atoms in the crystal lattice and excites them. After that these excited atoms re-emit the absorbed energy in the form of light as they return to the ground state. The passing particle creates an electromagnetic shower, and the amount of light emitted by the crystal is proportional to the energy of the incident particle[6].

6. K-long and Muon Detector

   The KLM detector helps in the detection of high momentum muons and neutral K_L^0 mesons.The KLM is composed of thick iron plates and Resistive Plate Chambers (RPC). When a charged particle passes through the gas element of the RPC, it ionizes it. The high electric field causes electrons to cause more ionization, creating a streamer between the electrodes. The streamer is picked up by the readout strips on either side of the chamber for further analysis[7].

Chapter 2

Search for the Dark Photon

Dark Matter doesn't interact via the electromagnetic forces. As there are no electromagnetic interactions, dark matter is invisible. According to the data collected by the Planck, the observed Universe consists of 26.8% of dark matter, 68.3% of dark energy and 4.9% of ordinary matter[8]. By the end of 19th century, new images from astronomical photography, unfold dark regions in the sky. From the pictures, scientists found that stars aren′t evenly distributed.

2.1 Observational Evidence of Dark Matter

2.1.1 Galaxy Clusters

A Swiss-American astronomer Fritz Zwicky studied the Coma galaxy cluster, and he determined that it did not contain enough visible matter to hold itself together. He studied around 800 galaxies in the cluster and expected to have a velocity dispersion of 80 kilometers per second, but he found that the real value was approximately equal to 1,000 kilometers per second. That stars were traveling at such a high speed that they should escape their mutual gravitational pull. Dark matter may be the material that is quietly holding the galaxy clusters tightly together[9].

2.1.2 Galactic Rotation curves

Rotation curve of a star in the galaxy is the graph of its velocity versus its distance from the center of the galaxy. From the rotational curves of stars in the galaxy, an astronomer can deduce the mass distribution. Based on Newtonian dynamics we expect the stars that are farther away from the galactic center move slower than the

stars near the center. That means the velocity of object decrease as the distance from the galactic center increases. Later Ford and Rubin discovered that instead of sloping down the rotation curves seemed to level off. This shape implies that the velocities of stars lying at large radii were moving with the same velocity of stars near the center. The galaxy should provide enough gravity to hold these fast-moving stars together. The observed, visible mass of a galaxy is not sufficient to provide required gravity. Therefore, scientists concluded that galaxies contain enormous dark matter. The addition of dark matter gives an excellent fit to the data taken for drawing the galactic rotation curve[10].

2.1.3 Gravitational Lensing

According to Einstein′s General Theory of Relativity, massive objects can act as a lens to bend the light. This property of massive object helps to confirm dark matter existence even though it emits no light. The gravitational field of a massive object makes the light rays passing close to that object bent and refocused somewhere else. Sometimes, light coming from more distant galaxies that pass close to a cluster may be distorted by its mass. In some cases, gravitational lensing led to the formation of multiple images of the same galaxy. There exist dark matter in between earth and the distant galaxies. Though dark matter is invisible, it has mass. The light rays coming towards earth from distant galaxies will pass through the gravitational field of dark matter and hence will be bent by the lensing effect[10].

2.1.4 The Cosmic Microwave Background

Astrophysicists believe that a very dense mixture of protons, neutrons, photons, electrons, and other subatomic particles filled the universe following the Big Bang. Atoms didn′t form as the temperature was so high. All the particles were in thermal equilibrium with each other. When universe expanded, the temperature falls to one billion degrees Kelvin (K). Atomic nuclei began to form at this temperature. Later the universe favored the formation of neutral hydrogen atoms when its temperature declined to 3000 K. After that, the universe became so transparent to photons. And photon is traveling throughout the universe since then. These relic photons form the cosmic microwave background (CMB).

Due to quantum mechanical fluctuations, there exist small variations in the density of both standard and dark matter. The dark matter and ordinary matter were

pulled towards the center of each swing by the gravity. Dark matter always move inwards due to gravitational pressure and normal matter move inwards only when the gravitational force overpowers the photon pressure otherwise normal matter will flow outward. When normal matter flow inwards it gets heated up else it gets cooled off. As the dark matter does not interact with photons, it is not affected by this ringing effect. As soon as the neutral hydrogen atoms were formed, the areas which contain matter were hotter than the areas which lack matter. Thus the information of the distribution of dark matter can be inferred from the temperature of the matter in different regions of the sky. Soon after the formation of neutral hydrogen, this pattern of temperature variations was frozen into the cosmic microwave background. The temperature variations in the CMB act as a map to find the location and amount of different types of matter. The accidental discovery of CMB occurred with the usage of the radio telescope.

It is inferred from the angular size and the extent of variation of CMB that the universe contained about five times as much dark matter as normal matter when the neutral hydrogen formed. Later, the details from supernovae and galaxy clusters are combined and reach a conclusion that dark energy comprises 73 percent of the universe, dark matter 23 percent, and normal matter just 4 percent[10].

2.2 Dark Photon

Dark Photons are hypothetical particles. Like photon in normal matter, a dark photon is the electromagnetic force carrier in the dark matter. It is believed that dark photon(A') has a weak coupling to the SM via kinetic mixing with the ordinary photon(γ) [11]. Non-SM particles may appear in some rare meson decays. Depending on their lifetimes, these particles may or may not appear as signals. The rare mesons decay into the dark photon with a highly suppressed branching ratio.

$$\mathcal{B}(X \to Y A') = \epsilon^2 \mathcal{B}(X \to Y \gamma) \tag{2.1}$$

where ϵ^2 carries a value lying between 10^{-6} and 10^{-8}. It is possible to reconstruct the masses of new light particles from the di-lepton invariant mass distribution[12].

2.3 Dark Photon Model-Kinetic Mixing Model

Kinetic mixing is a phenomenon in which a new gauge boson can change back and forth into the regular photon. Holdom proposed the kinetic mixing model, in which a dark photon could couple to normal matter. And this coupling is possible by introducing a loop of charged leptons, in between the Standard Model photon and the dark photon. This model consists of two unknown parameter

- Mass of the dark photon (m_γ).
- Mixing parameter (ϵ).

The mixing parameter parameterizes the strength of the coupling of the dark photon to the normal matter.

$$\epsilon^2 = \frac{\alpha'}{\alpha} \tag{2.2}$$

where α is the QED fine structure constant and α' is the dark coupling constant[13]. Some astrophysical observations suggest the existence of a dark photon in the GeV scale. Based on the kinematic mixing model, the dark photon has a mass on the MeV scale, and it is small compared to the dark matter particle. Therefore the decay of dark photon to dark matter particles is not possible. However, the dark photon decay to Standard Model particles (leptons and quarks), is suppressed by a factor of ϵ in comparison to the ordinary photon coupling[14].

2.4 Dark Photon Searches

The presence of dark photon is usually identified from two properties-displaced vertices and missing energy. After its production, the dark photon can decay either into the visible particles or DM particles. There are some advantages of probing DM particles at low energy e^+e^- colliders.

- Since production cross-section is inversely proportional to the center-of-mass energy (E_{cm}), the rate of production is large at low energy collider
- To detect rare events, high luminosity environment is favorable.
- The environment of a collider is clean and well controlled.

Some direct dark-photon production processes are shown in Figure 2.1.

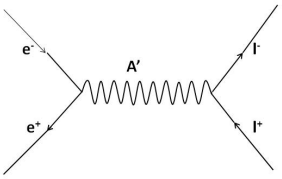

(a) $e^+e^- \to A'^*$

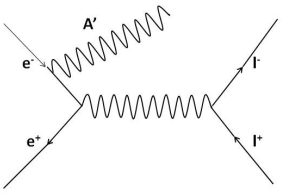

(b) $e^+e^- \to A'l^+l^-$

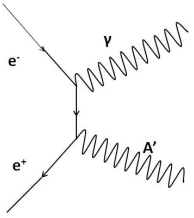

(c) $e^+e^- \to A'\gamma$

Figure 2.1: Direct dark photon prodution process at e^+e^- colliders

2.5 Anomaly in ^8Be Nuclear Transition

The Beryllium nucleus consists of 4 protons and 4 neutrons. An intense beam of the proton is impinged on thin ^7Li targets to produce excited Be nucleus. This result in the production of two resonant Beryllium states $^8Be^*$ having isospin 0 and $^8Be^{*0}$ having isospin 1. Most of the excited Beryllium decay back to proton and lithium ^7Li.

$$^8Be^* \to^7 Lip \tag{2.3}$$

Some of them decay through electromagnetic processes

$$^8Be^* \to^8 Be\gamma \tag{2.4}$$

If an electromagnetic decay has an energy greater than $2m_e$ then it is accompanied by a process involving internal pair conversion.

$$^8Be^* \rightarrow^8 Bee^+e^- \tag{2.5}$$

Radiative decay has a branching ratio of $\mathcal{B}(^8Be^* \rightarrow^8 Be\gamma) \approx 1.4 \times 10^{-5}$, and internal pair conversion has a branching ratio of $\mathcal{B}(^8Be^* \rightarrow^8 Bee^+e^-) \approx 5.5 \times 10^{-8}$. In case of the internal pair conversion (IPC), the opening angle(θ) between e^+ and e^- ,and the invariant mass m_{e^+e} is measured. Normally these types of distribution show a peak at low values of θ and m_{e^+e} and then fall smoothly and monotonically for increasing values. Instead of this, there are pronounced bumps at $\theta \approx 140^0$ and at $m_{e^+e^-} \approx 17$ MeV. The excess is seen only in the case of the $^8Be^*$ resonance and $^8Be^{*0}$ IPC decays don't show any bumps. Excess appears only for symmetric electron-positron pairs, which is expected in case of an intermediate massive particle. The peaks in angular and invariant mass distributions match. This suggest for a new boson $X(16.7)$ that is produced on-shell[15].

$$^8Be^* \rightarrow^8 BeX \tag{2.6}$$

$$X(16.7) \rightarrow e^+e^- \tag{2.7}$$

Usually, a dark photon would couple to electrons and protons, and it is found that the new boson X would couple only to electrons and neutrons. Therefore, the new boson is named as "protophobic X-boson". Since its energy is too high to be a dark photon, it as named as "protophobic X-boson". Though the new boson has no connection with the DM, one can expect it in $D^{*0} \rightarrow D^0e^+e^-$ decay. This is based on a very naiive expectation :

$$\frac{\mathcal{B}(D^{*0} \rightarrow D^0X(16.7))}{\mathcal{B}(D^{*0} \rightarrow D^0\gamma))} \sim \frac{\mathcal{B}(^8Be^* \rightarrow^8 BeX(16.7))}{\mathcal{B}(^8Be^* \rightarrow^8 Be\gamma))} \sim 5.8 \times 10^{-6} \tag{2.8}$$

One can look for "Protophobic X-boson" in the D^{*0} decay.

2.6 Signal

One can search for the dark photon from the charm meson decay at LHCb[11]. This search is not easy in Belle due to the low momentum electron tracks. The current study will provide crucial information regarding the Belle(II) capabilities for the dark

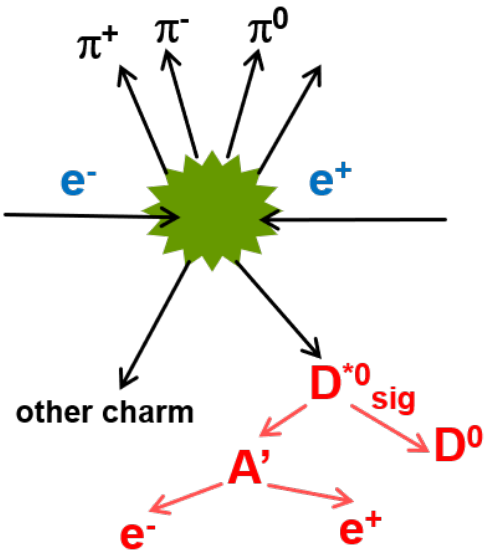

Figure 2.2: Production process of hypothetical dark photon in D^{*0} decay at e^+e^- collider.

photon search in D^{*0} meson decay. As shown in Figure 2.2, the electron and positron beam collides and produce $c\bar{c}$ which fragment and one c-quark gaves D^{*0} and then D^0 decay. The signal is highlighted with the red colour.
To reconstruct $D^{*0} \to D^0 X(\to e^+e^-)$ decay mode, we first reconstruct D^0 particle and then combine it with two oppositely charged electron tracks to make D^{*0}.
Signal is identified using the following variables:

1. $\mathbf{M(D^0)}$, invariant mass of D^0
2. $\mathbf{\Delta M}$, mass difference between D^{*0} and D^0 candidates, $\Delta M = M(D^{*0}) - M(D^0)$.
3. $\mathbf{M_{e^+e^-}}$, invariant mass of e^+ and e^- candidates.
4. $\mathbf{p^*_{D*}}$, momentum of D^{*0} in CM frame.

Fig. 2.3 shows the above mentioned distributions used to identify the signal. Signal window is defined as $0.1425 < \Delta M < 0.1480$ GeV/c^2 and $1.85 < M_{D^0} < 1.88$ GeV/c^2. To suppress the background due to the D^* coming from B decays, we apply cut on $P^*_{D*} > 2$ GeV/c. Further, in order to increase our reconstruction efficiency, we used five decay of D^0 particles which makes up to $\sim 34\%$ of the total branching fraction of D^0 decay modes as mentioned in Table 2.1.

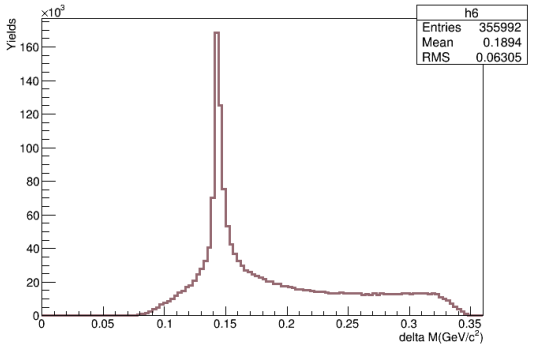

(a) ΔM distribution (GeV/c^2).

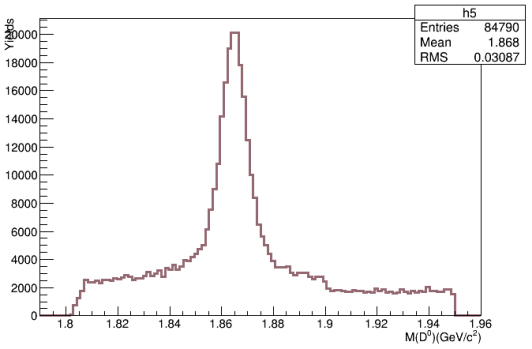

(b) M_{D^0} distribution (GeV/c^2).

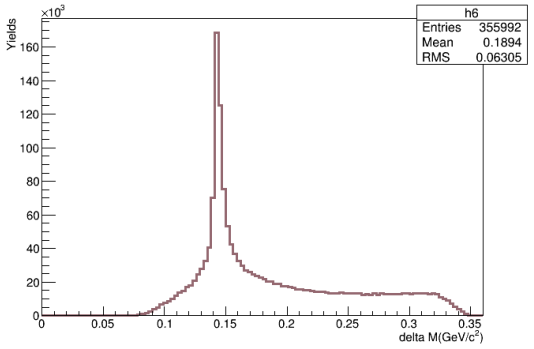

(c) $M_{e^+e^-}$ distribution (GeV/c^2) for the signal window.

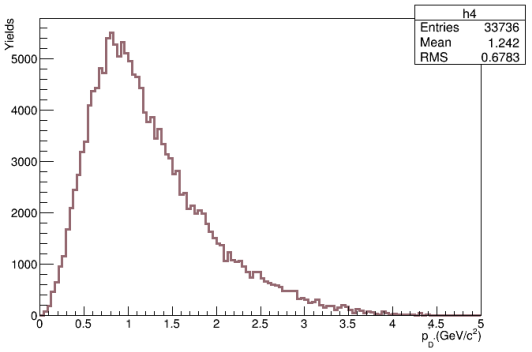

(d) $p^*_{D^*}$ distribution (GeV/c).

Figure 2.3: Used discriminating variables

D^0 decay	$\mathcal{B}$, in%
$K^-\pi^+$	3.9
$K^-\pi^+\pi^0$	13.9
$K^-\pi^+\pi^+\pi^-$	8.1
$K^0_s\pi^+\pi^-$	2.9
$K^0_s\pi^+\pi^-\pi^0$	5.4
Sum of all five modes	34.2

Table 2.1: D^0 Decay Modes and its branching fraction

2.7 Generic Monte Carlo Sample

In Belle, e^- beam having 8 GeV and e^+ beam having 3.5 GeV collide with each other at the $\Upsilon(4S)$ resonance. The $\Upsilon(4S)$ state is produced nearly along the z-axis of the KEKB asymmetric-energy collider. The $\Upsilon(4S)$ has an invariant mass of 10.58 GeV, which makes it to decay into a pair of B-mesons.

In its rest frame, $\Upsilon(4S)$ hadronises to a pair of B-mesons and is distributed spherically. As, it include charged (B^+-B^- pairs) and neutral(B^0-$\bar{B}^0$ paris) which we call charged and mixed events, respectively. Further e^+e^- collisions also result in production of $u\bar{u}$, $d\bar{d}$, $s\bar{s}$, and $c\bar{c}$ events. Such events are called continuum events. Here the light quark pairs created back-to-back have much more kinetic energy, which is approximately equal to the energy of the accelerator. As the hadrons produced are distributed near the axis of the e^+e^- collider, the continuum events are in a jet-like structure [16]. Table 2.2 shows all the generic decay events which occur at the interaction point.

Type	Production mode	Relative production (%)
Charged	$e^+e^- \to \Upsilon(4S) \to B^+B^-$	12
Mixed	$e^+e^- \to \Upsilon(4S) \to B^0\bar{B}^0$	12
charm	$e^+e^- \to c\bar{c}$	30
uds	$e^+e^- \to u\overline{u}/d\overline{d}/s\overline{s}$	46

Table 2.2: Generic MC sample explanation [1].

2.8 Data Analysis

2.8.1 Event Generation

We used EvtGen, an event generator, to generate the monte carlo (MC) signal events for our mode of interest. After that the response of the Belle detector is simulated using GEANT4(GEometry ANd Tracking).

EvtGen is a MC event generator that simulates the decays of B-mesons and other resonances. Here the generic decay table (Table 2.2) provides an extensive list of decays of particles. In addition to this, the output of EvtGen can be controlled via a user decay file[17]. We generated 1 Million signal MC sample for $e^+e^- \to c\bar{c}$ using EvtGen. Geant4 is a package for the simulation of particles passing through and interacting with matter, using montecarlo methods.

We prepared routine to reconstruct $D^{*0} \to D^0e^+e^-$ and $D^{*0} \to D^0X(25)[\to e^+e^-]$ using C++ in BASF environment. Figure 2.2 shows the artistic illustration of the process used to generate dark photon. D^0 is reconstructed from the decay modes mentioned in the Fig. 2.4 and combined with e^+ and e^- identified tracks. As we don't know the mass and width of the low mass hypothetical dark photon particle,we created dark photon candidate with zero width and different masses hypothesis: $X(16.7)$,

$X(25)$, $X(50)$, $X(75)$, $X(100)$, and $X(125)$. The masses inside the bracket are in MeV.

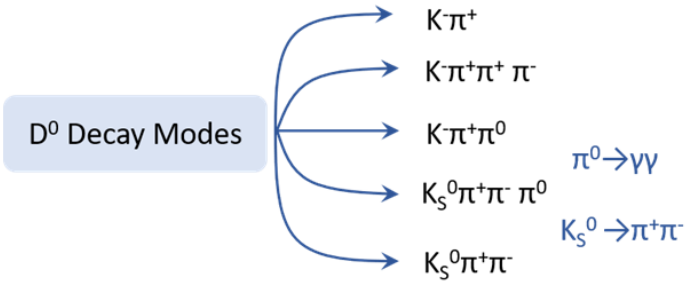

Figure 2.4: Used D^0 Decay Modes

2.8.2 Skimming

Data collected by Belle consists of a large number of events. Therefore, it takes a lot of time to run our reconstruction code. Further, if one need to modify the code, it takes more time again. To avoid wasting our computation resources, we did skim. As, there is no official skimming available for this analysis, we created our own skimming module.

Skimming is the process of generating a subset of raw data by applying some selection criteria. A code almost similar to reconstruction code (with loose cuts/criteria) is used for skimming, and it creates some index files, which contains pointer to the selected events[18]. For further analysis reconstruction code is run on the index files.

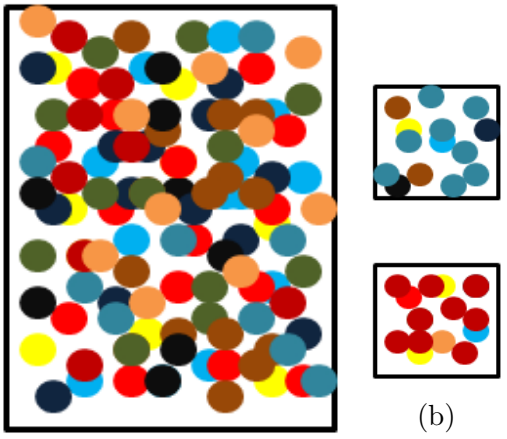

(a) Whole data set. (b) Skimmed data set.

Figure 2.5: Visualization of the whole data set.

Here color represents some particular events. As seen in whole data set, we have all the events. While in the skimmed data set we have only one color enhanced. Once the skimming is done, using skimmed data set is faster and saves computation resources along with time

2.9 Expected Background

In order to understand the background, we used the generic MC as explained in one of previous section. Using which, we identified the potential background sources. As per expectation, most of the background is coming from most D^* candidates not produced from the continuum events, but from $B \to D^* X$ decays. From the Figure 2.6 it is clear that most of the background is due to low momentum D^*.

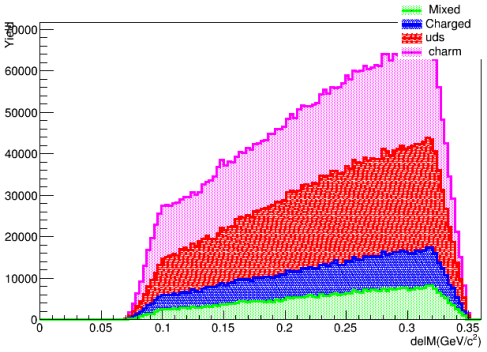

(a) ΔM distribution (GeV/c^2).

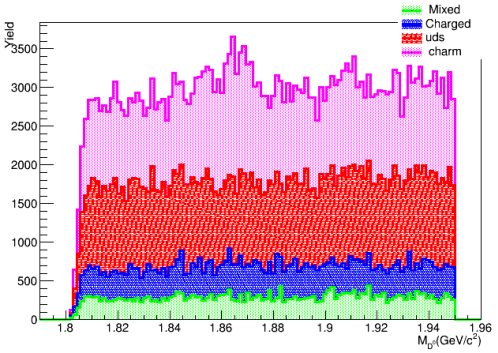

(b) M_{D^0} distribution (GeV/c^2).

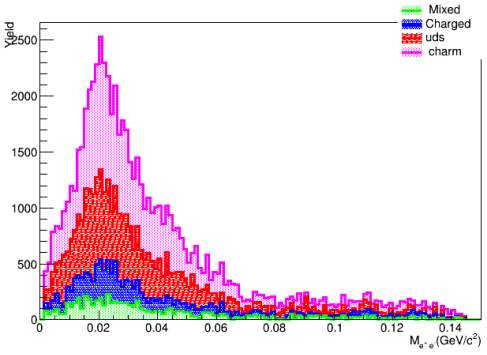

(c) $M_{e^+e^-}$ distribution (GeV/c^2) for the signal window..

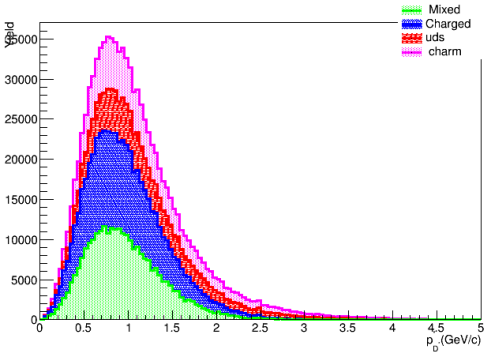

(d) $p^*_{D^*}$ distribution (GeV/c).

Figure 2.6: Expected background coming from generic MC sample.

2.10 Signal comparison with the background

We compared the expected background from generic sample with the signal generated.

1. $D^* \to D^0 e^+ e^-$

   The stacked plots of generic MC events, as well as signal, is made for each discriminating variables. In the case of signal, D^0 is reconstructed from our five decay modes. The following cuts are used to suppress the background :

   - $0.1425 < \Delta M < 0.1480$ GeV/c^2
   - $1.85 < M_{D^0} < 1.88$ GeV/c^2
   - $p^*_{D*} > 2$ GeV

   Since here e^+e^- don't come from any resonance (D^* decays to three body decay), the invariant mass of e^+e^- has a phase space distribution.

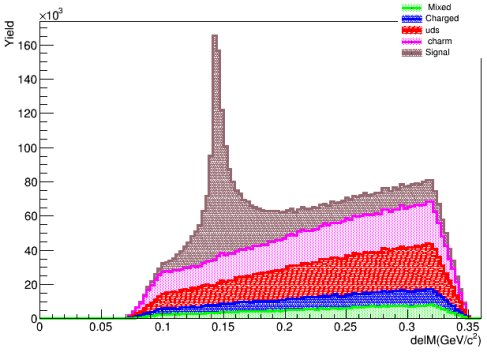

(a) ΔM distribution (GeV/c^2).

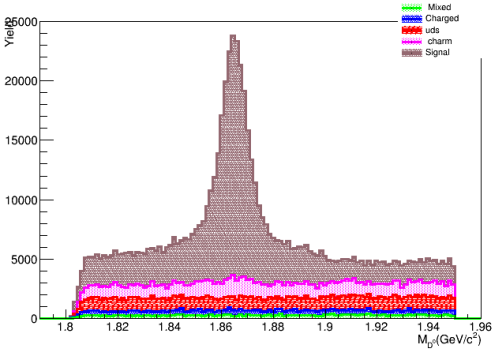

(b) M_{D^0} distribution (GeV/c^2).

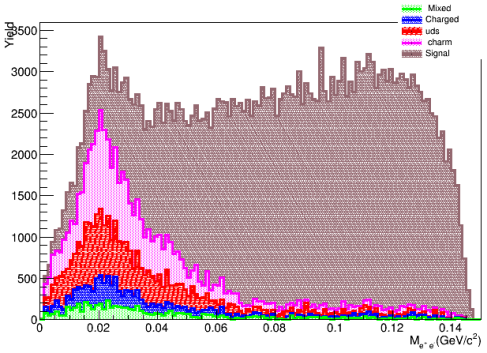

(c) $M_{e^+e^-}$ distribution (GeV/c^2) for the signal window.

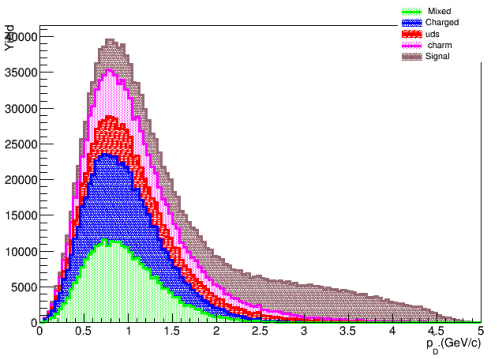

(d) $p^*_{D^*}$ distribution (GeV/c).

Figure 2.7: Signal and background plots for the decay $D^{*0} \to D^0 e^+ e^-$

2. $D^* \to D^0 X(25)[\to e^+e^-]$

   In order to verify that the cuts we used are fine for the case where e^+e^- comes from hypothetical dark photon resonance, we prepared stacked plots of generic MC events and signal MC of interest. Here also D^0 is reconstructed using the decay modes mentioned in Table 2.1. As expected, here we are see a clear invariant mass of e^+e^- at 25 MeV/c^2.

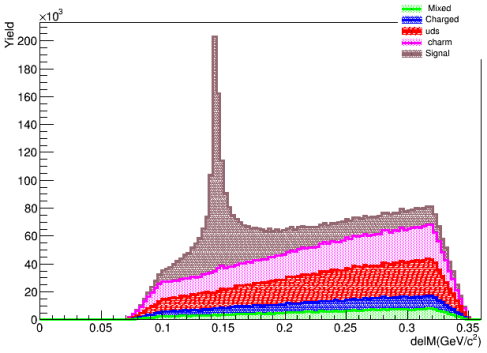

(a) ΔM distribution (GeV/c^2).

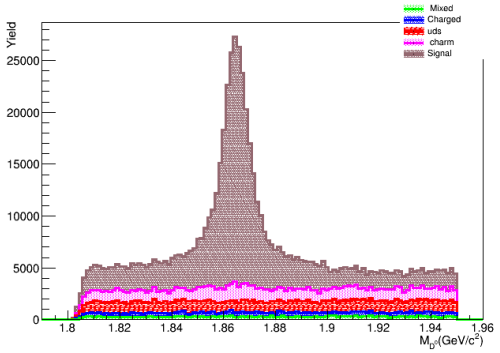

(b) M_{D^0} distribution (GeV/c^2).

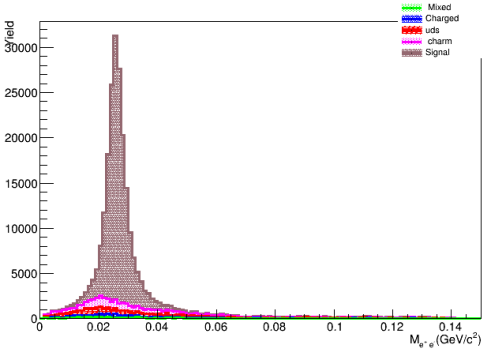

(c) $M_{e^+e^-}$ distribution (GeV/c^2) for the signal window..

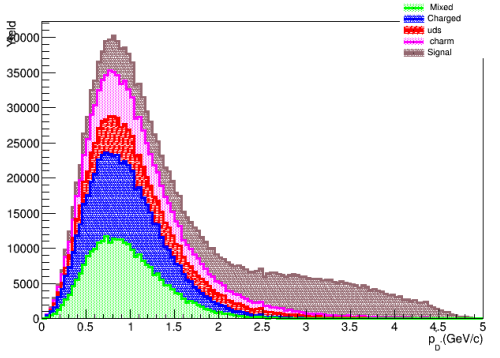

(d) $p^*_{D^*}$ distribution (GeV/c).

Figure 2.8: MC comparison $D^* \to D^0 X(25)[\to e^+e^-]$ decay mode.

2.11 Signal Efficiency

2.11.1 Fitting different D^0 decay modes

We used five D^0 decay modes for signal reconstruction. To know the signal reconstruction efficiency for different modes, we fit D^0 modes signal MC separately. From the estimated efficiency, we estimated the expected number of signal events one can expect. For this, we use the following:

- $\mathcal{B}(D^* \to D^0\gamma)$ as 35.3%.
- The branching fraction of each D^0 decay mode as provided in Table 2.1.
- Assumed D^* production (N_{D^*}) to be 10^9.
- Assumed ϵ^2 to be 10^{-6}.
- Asumed $\mathcal{B}(A' \to e^+e^-)$ to be 100%

One can estimate the expected signal to be :

$$N_{D^*} \times \epsilon^2 \times \mathcal{B}(D^* \to D^0\gamma) \times \mathcal{B}(D^* \to Kn\pi) \times \text{Efficiency} \tag{2.9}$$

Table 2.3 summarizes the expected yield of dark photons candidate for different D^0 modes.

Efficiency vs different D^0 decay modes has been plotted as Figure 2.10.

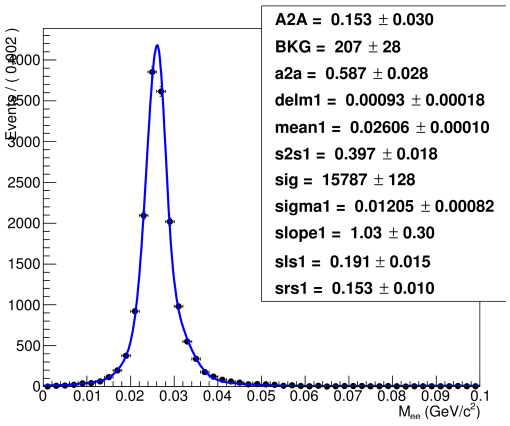

(a) $D^0 \to K^-\pi^+$ decay mode.

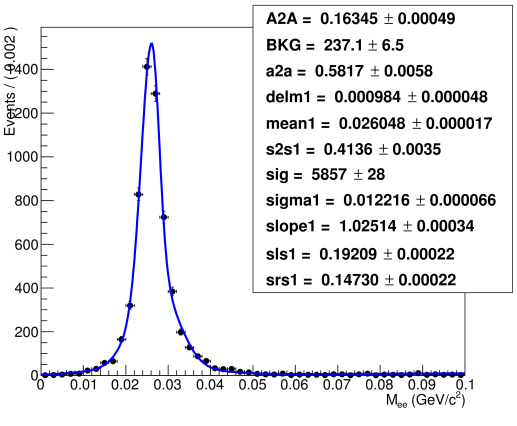

(b) $D^0 \to K^-\pi^+\pi^0$ decay mode.

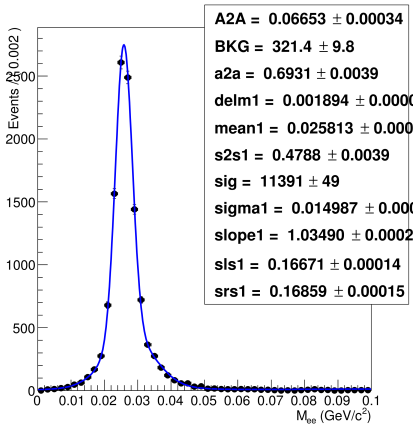

(c) $D^0 \to K^-\pi^+\pi^+\pi^-$ decay mode.

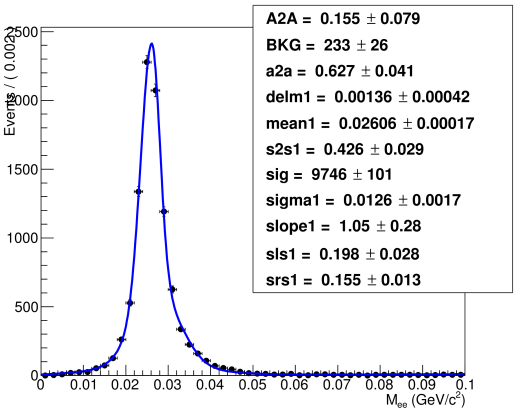

(d) $D^0 \to K^0_s\pi^+\pi^-$ decay mode.

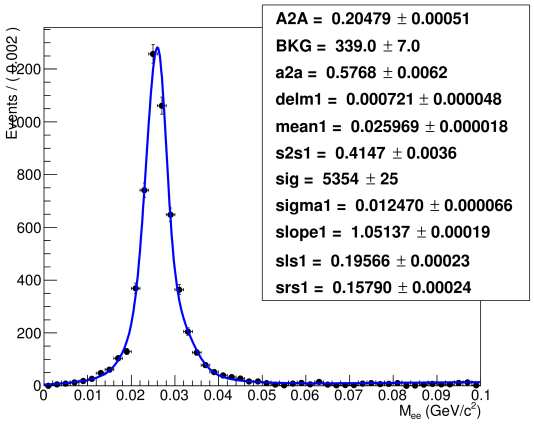

(e) $D^0 \to K^0_s\pi^+\pi^-\pi^0$ decay mode.

Figure 2.9: 1D fit to the $M_{e^+e^-}$ distribution for different D^0 decay modes in $D^* \to D^0X(25)$. To parameterize the signal PDF, we used sum of two Gaussians and a bifurcated Gaussian.

D^0 modes used for reconstruction	Efficiency (%)	$\mathcal{B}(D \to Kn\pi)(\%)$	Expected yield
$D^0 \to K^-\pi^+$	1.6	3.9	22
$D^0 \to K^-\pi^+\pi^0$	0.6	13.9	29
$D^0 \to K^-\pi^+\pi^+\pi^-$	1.1	8.1	33
$D^0 \to K^0_s\pi^+\pi^-$	1.0	2.9	10
$D^0 \to K^0_s\pi^+\pi^-\pi^0$	0.5	5.4	10

Table 2.3: Summarizing the expected yield of dark photons candidate for different D^0 modes using $\epsilon^2 \sim 10^{-6}$.

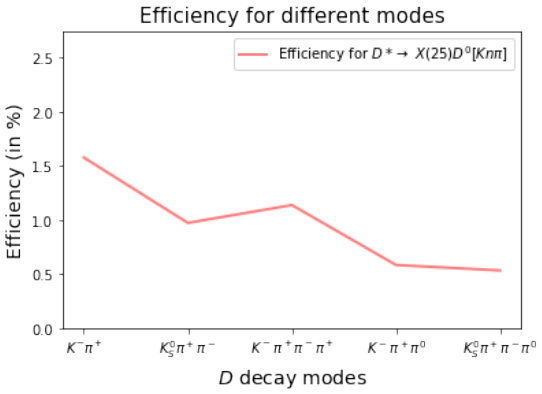

Figure 2.10: Efficiency (in %) vs D^0 decay modes.

2.11.2 Efficiency in variation with mass of dark photon.

In order to understand the effect of dark photon mass on efficiency, we generated dark photon with different mass hypothesis. For this purpose, we constraint ourself to $D^0 \to K^-\pi^+$ decay mode only. The dark photon mass was varied from 16.7 MeV to 125 MeV. We summarize the results form the fits to $M_{e^+e^-}$ as plot between efficiency and different A' masses (Figure 2.12). There is some variation in efficiency, but in large it is somewhat consistent. We found low mass region to have a little higher efficiency.

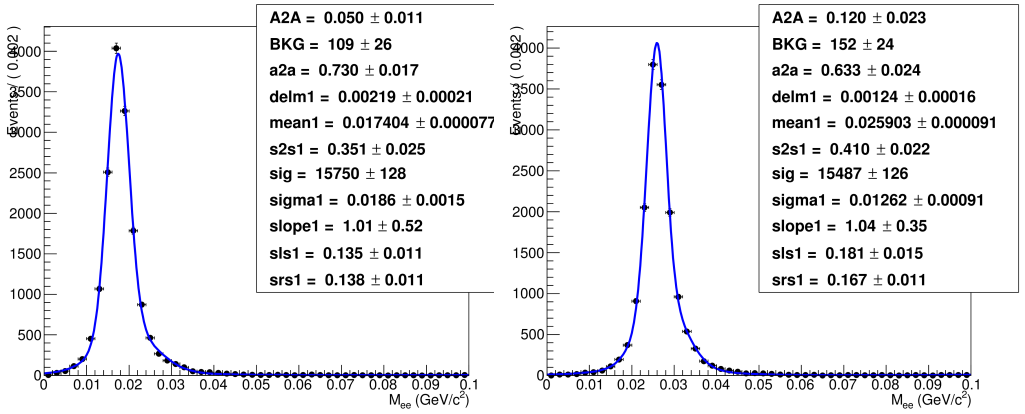

(a) $D^* \to D^0 X(16.7)$ decay mode. (b) $D^* \to D^0 X(25)$ decay mode.

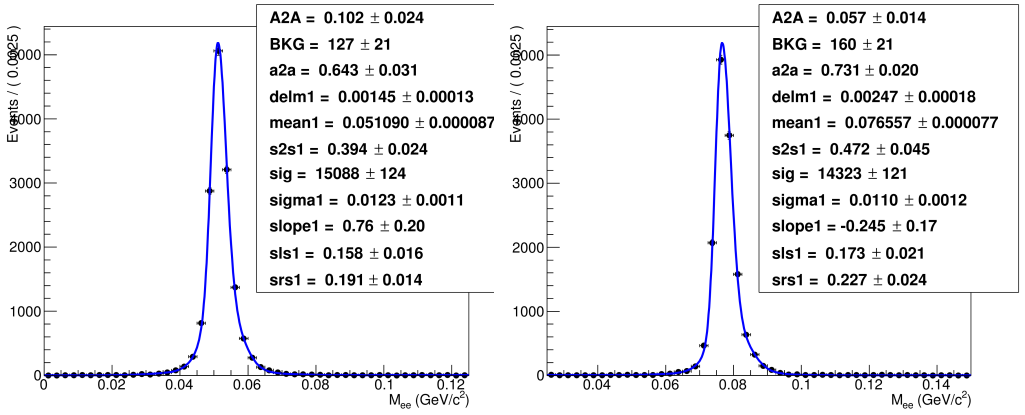

(c) $D^* \to D^0 X(50)$ decay mode. (d) $D^* \to D^0 X(75)$ decay mode.

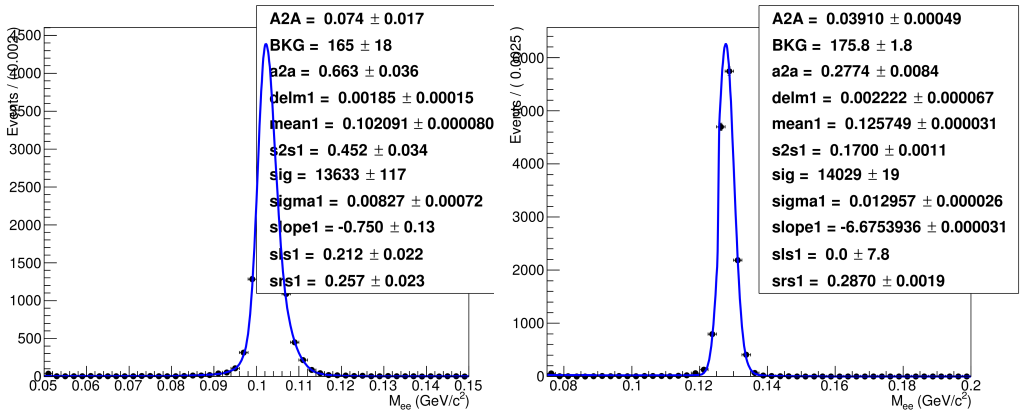

(e) $D^* \to D^0 X(100)$ decay mode. (f) $D^* \to D^0 X(125)$ decay mode.

Figure 2.11: 1D fit to the $M_{e^+e^-}$ distribution for different dark photon masses. To parameterize the signal PDF, we used sum of two Gaussians and a bifurcated Gaussian.

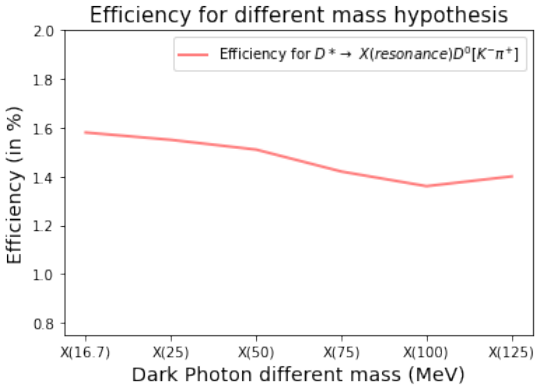

Figure 2.12: Efficiency (in %) vs different dark photon masses

Chapter 3

Low Momentum Muon Study at Belle II

3.1 Muons

The muon (μ) is an elementary particle. Its a spin 1/2 particle with charge -1e. It has a mass of 105.7 MeV/c^2. It is similar to an electron but about 200 times heavier than the electron. The muon is classified as a lepton in the SM. It′s very unstable and has a mean lifetime of about 2.2 μs [19] . The possible muon decays are shown in Figure 3.1.

$$\mu^- \rightarrow e^- \nu_e \nu_\mu \tag{3.1}$$

$$\mu^+ \rightarrow e^+ \nu_e \nu_\mu \tag{3.2}$$

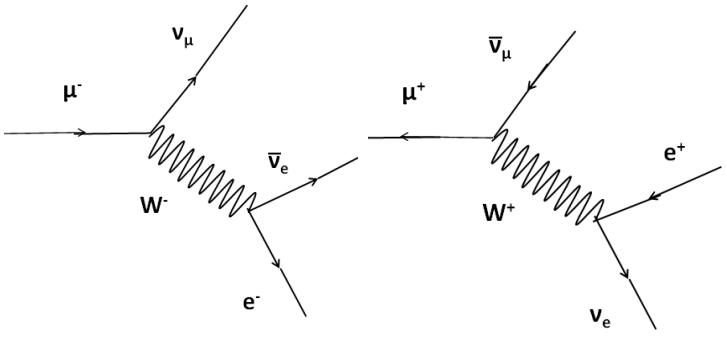

(a) μ^- decay to electron. (b) μ^+ decay to positron.

Figure 3.1: Muon decay feynman diagram.

In 1936, Carl Anderson and Seth Neddermeyer discovered muons. They were studying how the particles in a cosmic ray bent within an electromagnetic field. And they observed that negatively charged particles bent less sharply than electrons, but more sharply than protons, for the particle with the same velocity. This would mean that they must have been heavier particles than electrons, but smaller than protons. They published their findings in the New Evidence for the Existence of a Particle Intermediate Between the Proton and Electron [20].

3.2 Muon detection in Belle II

The interaction of muon with matter is small compared to other particles. Because of this reason, the muon can travel a considerable distance compared to others. Usually, in particle colliders, the muon detector is located in the outermost part. Likewise in Belle detector also the KLM detector, which detects muons, is situated on the surface portion. Therefore, only high momentum muons can reach there, and thus the low momentum muons remain undetected. Since low momentum muons are coming in contact with the inner sub-detectors, the observables from these detectors can be used for the muon detection.

3.3 Importance of low momentum muon study

- **Flavour-Changing Neutral Current(FCNC)**
  The flavor-changing neutral current process is the process in which the flavor of a fermion current change without altering its electric charge [21]. It may happen in the SM beyond the tree level, but they are highly suppressed by the GIM mechanism. The theories that attempt to go beyond the SM predicts FCNCs such as B-meson semileptonic decay:

$$B \to K l^+ l^- \tag{3.3}$$

  These decays are suppressed as the NP particles can contribute anomalies in their SM estimation. To measure the anomalies with precision, one needs to study these decay modes at high luminosity. In this decay, one expects to have low momentum muons, which is crucial for improvement in the $R_{K^{(*)}}$ anomalies. Consider the ratio of branching fraction of B-meson decay to K-meson, e^+ and e^- to that of B-meson decay to K-meson, μ^+ and μ^-. If we plot the ratio

of their branching fraction along their momentum, one find anomalies between SM and data at low q^2. Improvement in low momentum muon detection will help in improving the efficiency and in the end help in doing a more precise measurement.

- **Lepton Flavour Violation(LFV)**
  According to the SM, lepton number is conserved in an elementary reaction. Lepton number is defined as the difference between the number of leptons and the number of antileptons. LFV indicates the decay in which lepton number isn′t conserved. Its observation would be a definite sign for NP beyond the SM. One such decay is the rare decay of tau particle.

$$\tau^+ \rightarrow \mu^-\mu^+\mu^- \tag{3.4}$$

  In this decay the tau number and muon number aren't conserved. Since the final products include three muons, there may be a chance of production of low momentum muon in the final state.

Improvement in low momentum muons detection efficiency will increase the signal sensitivity to NP processes.

3.4 Study

Signals were generated for different particles (e, μ, γ, K, and π) using particle gun with different energies ranging from 100 MeV to 500 MeV using BASF2 environment. Then we search for the possible variables, which one can use to identify and distinguish different particles.

3.4.1 Variables Used

Energy deposited in PXD

PXD is the innermost detector. Energy deposited in PXD for different particles and different momenta are plotted. The Kaon particle peaks at high energy values compared to others. It is due to the interaction of K is high compared to another particle. As the interaction is high, it deposits more energy compared to others.

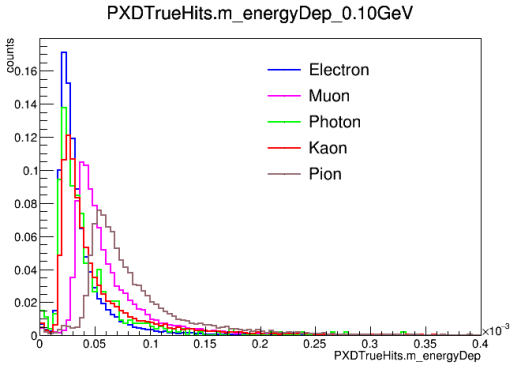

(a) 100 MeV energetic particle.

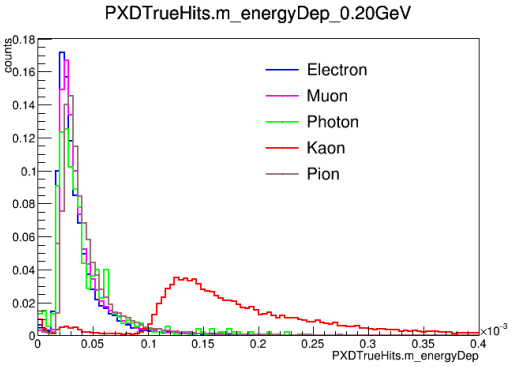

(b) 200 MeV energetic particle.

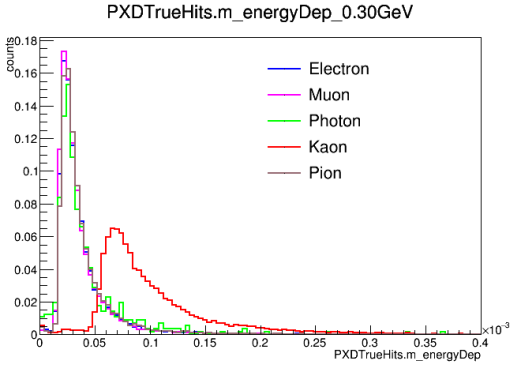

(c) 300 MeV energetic particle.

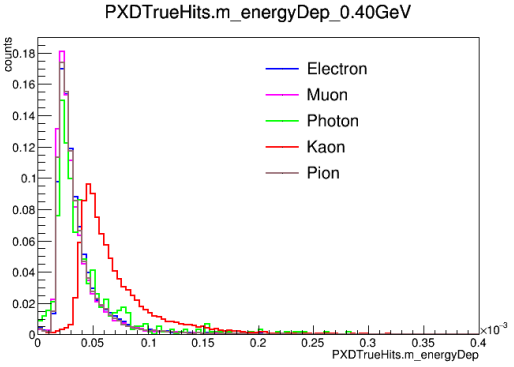

(d) 400 MeV energetic particle.

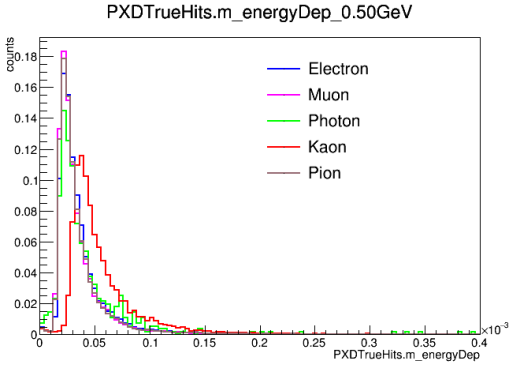

(e) 500 MeV energetic particle.

Figure 3.2: PXD Energy Deposited at different energies

Cluster charge in SVD

SVD detector consists of four layers. The accumulation of charge from all the four layers form the cluster charge.

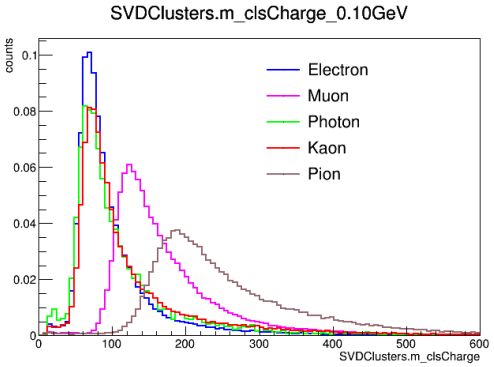

(a) 100 MeV energetic particle.

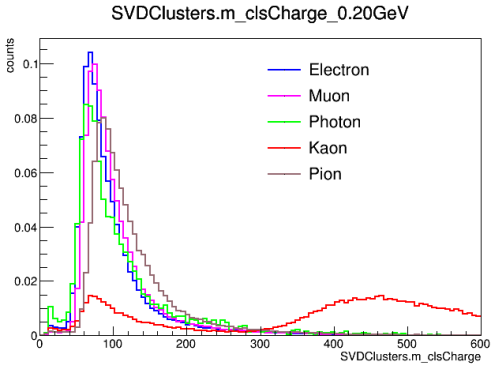

(b) 200 MeV energetic particle.

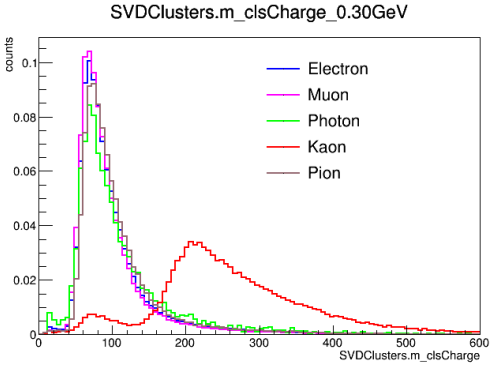

(c) 300 MeV energetic particle.

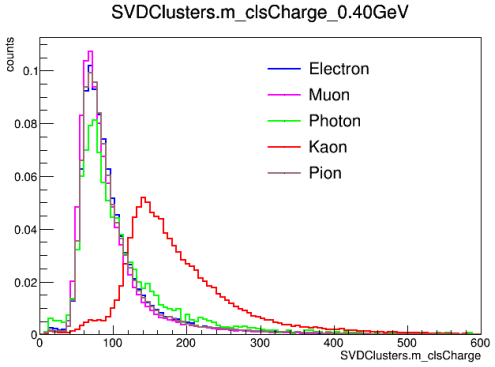

(d) 400 MeV energetic particle.

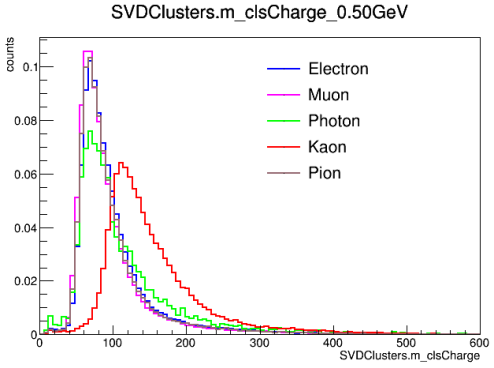

(e) 500 MeV energetic particle.

Figure 3.3: SVD cluster charge at different energies

ADC counts in CDC

Energy deposited in the CDC is stored as ADC counts. Here the pion shows a deviation from other plots at 100 MeV.

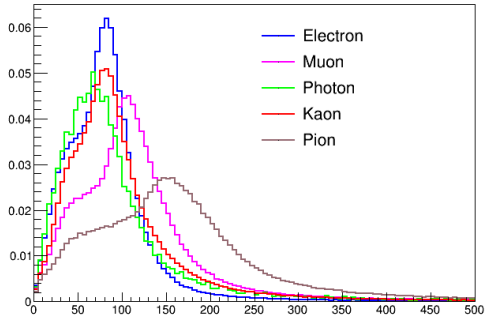

(a) 100 MeV energetic particle

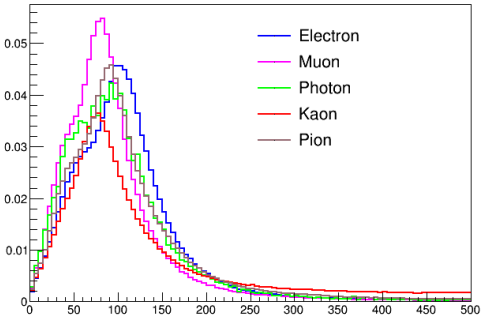

(b) 200 MeV energetic particle

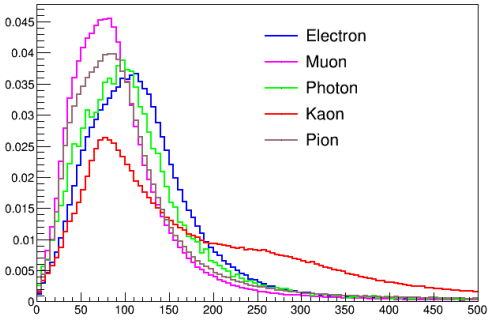

(c) 300 MeV energetic particle

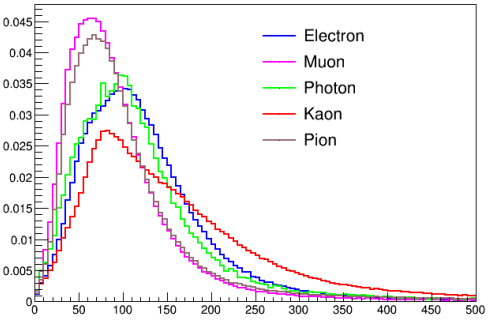

(d) 400 MeV energetic particle

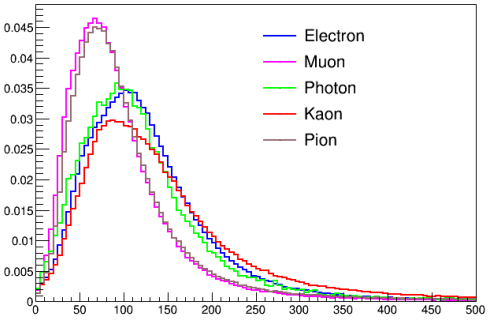

(e) 500 MeV energetic particle

Figure 3.4: CDC ADC count at different energies

Chapter 4

Results and Conclusions

Thesis work can be divided into two parts:

- Search for the dark photon
  - Generate signal MC for $D^* \to D^0 A'(\to e^+e^-)$ using EvtGen and GSIM.
  - Efficiency is estimated for different D^0 modes used for reconstruction : $K^-\pi^+$, $K^-\pi^+\pi^0$, $K^-\pi^+\pi^+\pi^-$, $K^0_S\pi^+\pi^-$, and $K^0_S\pi^+\pi^-\pi^0$.
  - Different mass hypothesis was used and efficiency was estimated to be almost similar.
  - Signal events expected for dark photon using the low ϵ^2 value (kinetic mixing value), which is maximum possible $\mathcal{B}(D^* \to D^0 A')$, results in 100 signal events using the full Belle data.
  - Background is also estimated using the generic MC sample.
  - Skim has been done for this mode. This will help in studying this the mode in future.
  - From the preliminary study, this decay mode seems to constraint the dark photon kinetic mixing model.
- Low momentum muon study
  - Generate different particles (e, μ, K, π and γ with different energies using the particle gun in the BASF2 framework.
  - Reconstructed the particle and studied its properties in different detectors.
  - Found energy deposited in the PXD, SVD cluster charge and CDC ADC counts to be useful in order to recover the low momentum muon particles.

– Using them, one expect to improve the particle identification for low momentum muons.

4.1 Future scope

- Currently, we take all the combinations as our signal/background. One needs to reduce the multiple candidates and perform the best candidate selection.
- Optimzation of the cuts/criteria for different D^0 modes to suppress the background.
- Identify the broad peaking-like structure in $M_{e^+e^-}$ and reduce it.
- Use all the streams to verify the background understanding.
- Data sideband of M_{D^0} and ΔM to verify/fix the background in $M_{e^+e^-}$.
- Do a more precise calculation of the constraint one can have on the kinetic mixing model.
- Search for more variables for low momentum muons in the Belle II.
- Do multivariate analysis for muon identification.

Appendix A

Signal and Background comparison for $D^* \to D^0 e^+ e^-$ and $D^* \to D^0 X(25)[\to e^+ e^-]$

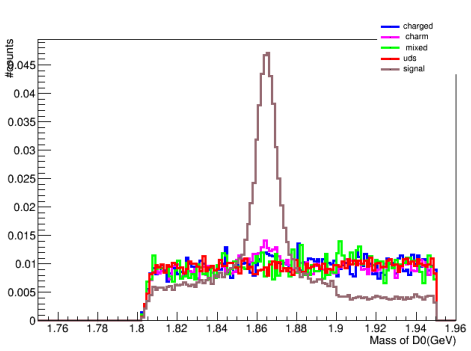

(a) M_{D^0} distribution for $D^* \to D^0 e^+ e^-$

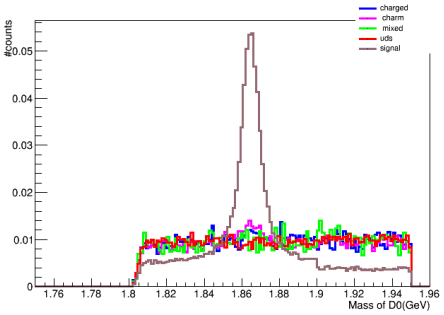

(b) M_{D^0} distribution for $D^* \to D^0 X(25)[\to e^+ e^-]$

Figure A.1: Invariant mass (M_{D^0}) distribution for $D^* \to D^0 n\pi$

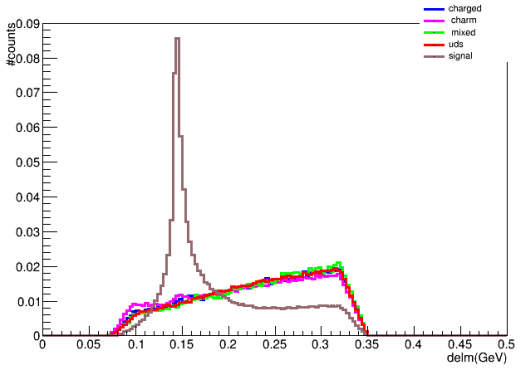

(a) ΔM distribution for $D^* \to D^0 e^+ e^-$

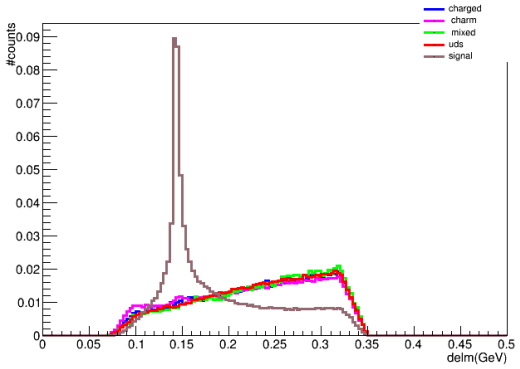

(b) ΔM distribution for $D^* \to D^0 X(25)[\to e^+ e^-]$

Figure A.2: Mass Difference($\Delta M \equiv M_{D^*} - M_{D^0}$)distribution for $D^* \to D^0 n\pi$

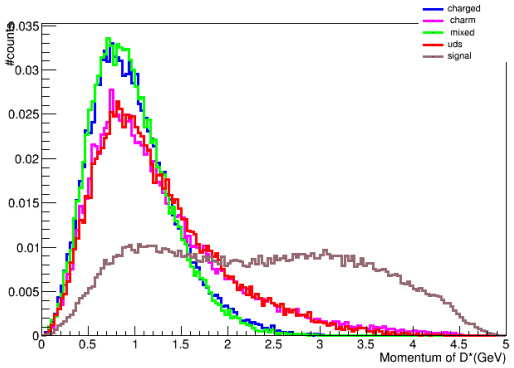

(a) p_{D^*} distribution for $D^* \to D^0 e^+ e^-$

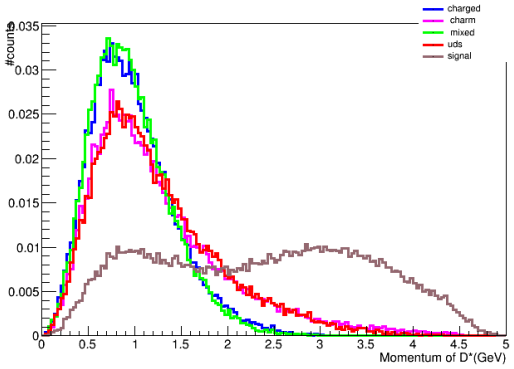

(b) p_{D^*} distribution for $D^* \to D^0 X(25)[\to e^+ e^-]$

Figure A.3: p_{D^*} distribution for $D^* \to D^0 n\pi$

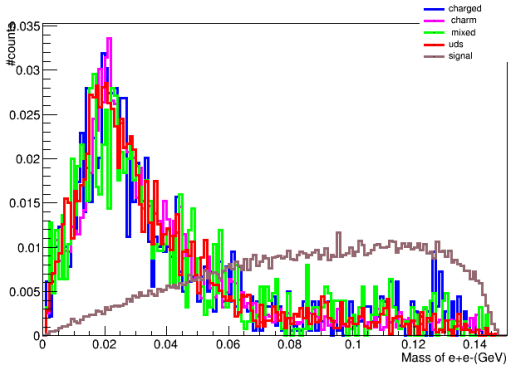

(a) $M_{e^+e^-}$ distribution for $D^* \to D^0 e^+ e^-$

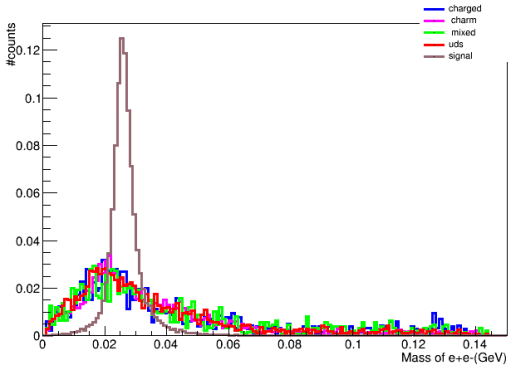

(b) $M_{e^+e^-}$ distribution for $D^* \to D^0 X(25)[\to e^+e^-]$

Figure A.4: $M_{e^+e^-}$ distribution for $D^* \to D^0 n\pi$

Appendix B

B.1 ΔM , M_{D^0}, and $M_{e^+e^-}$ distribution for different D^0 decay modes

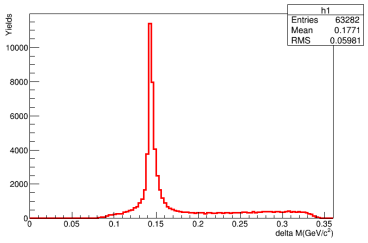

(a) ΔM distribution in GeV/c^2

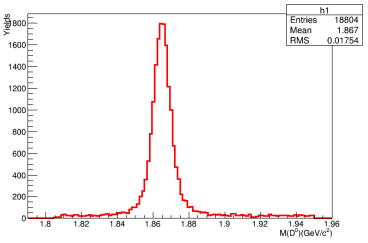

(b) M_{D^0} distribution in GeV/c^2

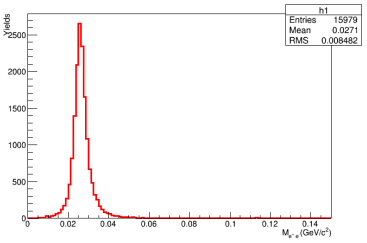

(c) $M_{e^+e^-}$ distribution in GeV/c^2

Figure B.1: $D^0 \to K^-\pi^+$ Signal MC

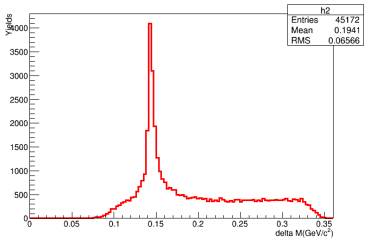

(a) ΔM distribution in GeV/c^2

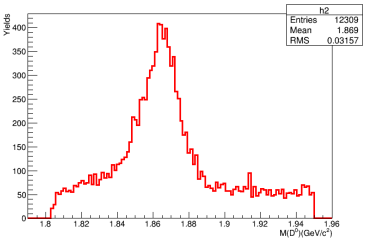

(b) M_{D^0} distribution in GeV/c^2

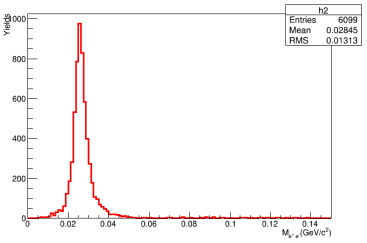

(c) $M_{e^+e^-}$ distribution in GeV/c^2

Figure B.2: $D^0 \to K^-\pi^+\pi^0$ Signal MC

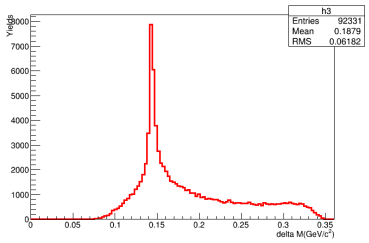

(a) ΔM distribution in GeV/c^2

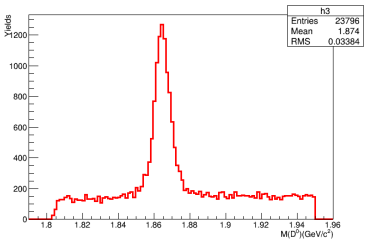

(b) M_{D^0} distribution in GeV/c^2

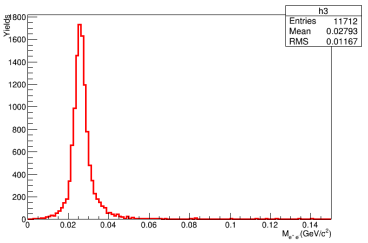

(c) $M_{e^+e^-}$ distribution in GeV/c^2

Figure B.3: $D^0 \to K^-\pi^+\pi^+\pi^-$ Signal MC

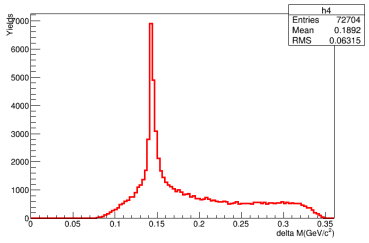

(a) ΔM distribution in GeV/c^2

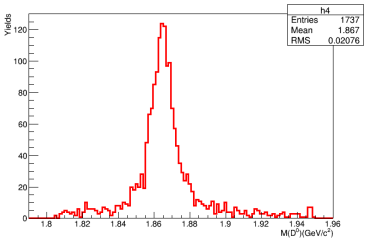

(b) M_{D^0} distribution in GeV/c^2

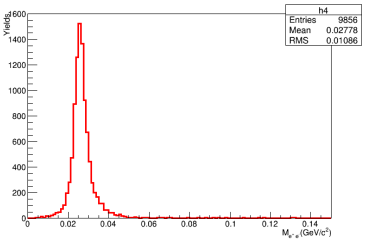

(c) $M_{e^+e^-}$ distribution in GeV/c^2

Figure B.4: $D^0 \to K^0_s\pi^+\pi^-$ Signal MC

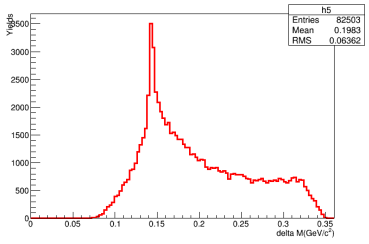

(a) ΔM distribution in GeV/c^2

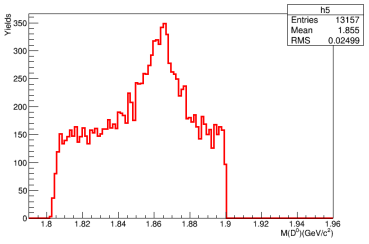

(b) M_{D^0} distribution in GeV/c^2

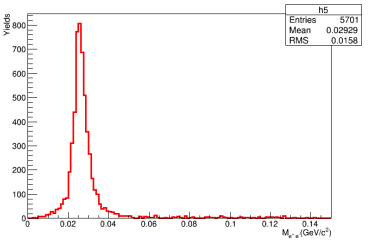

(c) $M_{e^+e^-}$ distribution in GeV/c^2

Figure B.5: $D^0 \to K^0_s\pi^+\pi^-\pi^0$ Signal MC

Appendix C

(M_{ee}) distribution for signal and Background

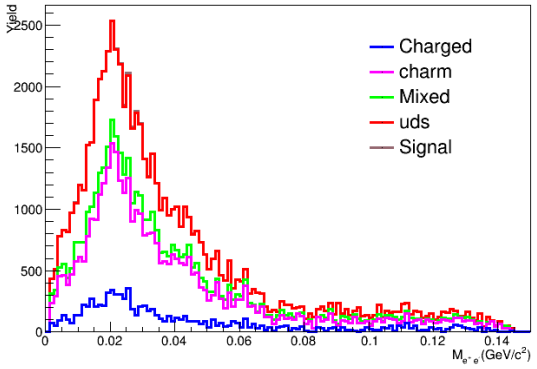

Figure C.1: Invariant mass (M_{ee}) distribution for different D^0 decay modes along with the expected signal and the background

Bibliography

[1] O. Lutz, *Search for $B \to h(*)\nu\bar{\nu}$ Decays at Belle and Development of Track Finding for Belle II*. PhD thesis, KIT, Karlsruhe, 2012.

[2] G. Sciolla, "The mystery of cp violation," *MIT PHYSICS ANNUAL*, 2006.

[3] Y. Liu, "Methods on local hit reconstruction in the pixel detector for the belle ii experiment," 2013. Karlsruher Institut f r Technologie (KIT), Diplomarbeit, 2013.

[4] F. Mueller, "Some aspects of the Pixel Vertex Detector (PXD) at Belle II," *JINST*, vol. 9, no. 10, p. C10007, 2014.

[5] S. Sandilya, "Particle Identification with the TOP and ARICH detectors at Belle II," in *22nd DAE-BRNS High Energy Physics Symposium Delhi, India, December 12-16, 2016*, 2017.

[6] A. Fodor and A. Warburton, *Design and Simulation of Beam-Background Monitors in the Vicinity of the Electromagnetic Calorimeter for the Belle II Experiment*. PhD thesis, Montreal, McGill University, Montreal, 2017. Presented on 23 03 2017.

[7] T. Abe *et al.*, "Belle II Technical Design Report," 2010.

[8] R. Kuhtz, *Physical science*. New York: Britannica Educational Publishing in association with Rosen Educational Services, 2017.

[9] S. van den Bergh, "The Early history of dark matter," *Publ. Astron. Soc. Pac.*, vol. 111, p. 657, 1999.

[10] K. Freese, "Review of Observational Evidence for Dark Matter in the Universe and in upcoming searches for Dark Stars," *EAS Publ. Ser.*, vol. 36, pp. 113–126, 2009.

[11] P. Ilten, J. Thaler, M. Williams, and W. Xue, "Dark photons from charm mesons at LHCb," *Phys. Rev.*, vol. D92, no. 11, p. 115017, 2015.

[12] P.-F. Yin and S.-H. Zhu, "Light dark sector searches at low-energy high-luminosity e + e colliders," *Frontiers of Physics*, vol. 11, p. 111403, Apr 2016.

[13] Denig, Achim, "Review of dark photon searches," *EPJ Web Conf.*, vol. 130, p. 01005, 2016.

[14] A. Denig, "Low-Energy Tests of the Standard Model - $(g-2)_\mu$ and Dark Photons," in *Proceedings, 20th International Conference on Particles and Nuclei (PANIC 14): Hamburg, Germany, August 24-29, 2014*, pp. 52–63, 2014.

[15] J. L. Feng, B. Fornal, I. Galon, S. Gardner, J. Smolinsky, T. M. P. Tait, and P. Tanedo, "Protophobic fifth-force interpretation of the observed anomaly in ^{8}Be nuclear transitions," *Phys. Rev. Lett.*, vol. 117, p. 071803, Aug 2016.

[16] D. Weyland, "Continuum Suppression with Deep Learning techniques for the Belle II Experiment," Master's thesis, KIT, Karlsruhe, ETP, 2017-11-02.

[17] A. Ryd, D. Lange, N. Kuznetsova, S. Versille, M. Rotondo, D. P. Kirkby, F. K. Wuerthwein, and A. Ishikawa, "EvtGen: A Monte Carlo Generator for B-Physics," 2005.

[18] N. Nellikunnummel, *Search for CP violation and rare decays in neutral charm mesons at Belle*. PhD thesis, Aligarh Muslim U., 2009.

[19] Wikipedia contributors.

[20] K. D. Bruyn, "Lepton flavour violation in tau decays: Results and prospects at the lhc," *Nuclear and Particle Physics Proceedings*, vol. 287-288, pp. 164 – 167, 2017. The 14th International Workshop on Tau Lepton Physics.

[21] Wikipedia contributors.

[22] S. Anderson *et al.*, "Improved upper limits on the FCNC decays $B \to K\ell^+\ell^-$ and $B \to$ K*(892) $\ell^+\ell^-$," *Phys. Rev. Lett.*, vol. 87, p. 181803, 2001.

[23] D. Ghosh, "Explaining the R_K and R_{K^*} anomalies," *Eur. Phys. J.*, vol. C77, no. 10, p. 694, 2017.